Assimilation of Vegetation Conditions Improves the Representation of Drought over Agricultural Areas

DAVID M. MOCKO,[a] SUJAY V. KUMAR,[b] CHRISTA D. PETERS-LIDARD,[c] AND SHUGONG WANG[a]

[a] *Science Applications International Corporation, Hydrological Sciences Laboratory, NASA Goddard Space Flight Center, Greenbelt, Maryland*
[b] *Hydrological Sciences Laboratory, NASA GSFC, Greenbelt, Maryland*
[c] *Earth Sciences Division, NASA GSFC, Greenbelt, Maryland*

(Manuscript received 4 March 2020, in final form 25 November 2020)

ABSTRACT: This study presents an evaluation of the impact of vegetation conditions on a land surface model (LSM) simulation of agricultural drought. The Noah-MP LSM is used to simulate water and energy fluxes and states, which are transformed into drought categories using percentiles over the continental United States from 1979 to 2017. Leaf area index (LAI) observations are assimilated into the dynamic vegetation scheme of Noah-MP. A weekly operational drought monitor (the U.S. Drought Monitor) is used for the evaluation. The results show that LAI assimilation into Noah-MP's dynamic vegetation scheme improves the model's ability to represent drought, particularly over cropland areas. LAI assimilation improves the simulation of the drought category, detection of drought conditions, and reduces the instances of drought false alarms. The assimilation of LAI in these locations not only corrects model errors in the simulation of vegetation, but also can help to represent unmodeled physical processes such as irrigation toward improved simulation of agricultural drought.

KEYWORDS: North America; Drought; Vegetation; Soil moisture; Data assimilation; Land surface model

1. Introduction

Estimates of terrestrial water budget components from land surface models (LSMs) are routinely used in drought monitoring and forecasting environments (e.g., Mo et al. 2011; Houborg et al. 2012; Hao et al. 2014; Sheffield et al. 2014). In particular, Land Data Assimilation Systems (LDASs), which employ LSMs forced with observed meteorology, are used for operational drought monitoring at continental and global scales. The North American Land Data Assimilation System (NLDAS; Xia et al. 2012, 2014) is such an environment, which runs four separate LSMs driven with the same high-quality meteorological data, including a gauge-based precipitation analysis and bias-corrected radiation. The near-real-time NLDAS drought monitor (Ek et al. 2011; Sheffield et al. 2012) provides several indices of drought estimates based on anomalies and percentiles of precipitation, soil moisture, streamflow, snow, and evapotranspiration. These drought indices represent the departure of the current state of the variable of interest relative to the long-term average.

Despite the stated emphasis, most near-real-time LDAS environments only include limited assimilation of terrestrial hydrological observations. Several recent efforts have focused on mitigating this limitation in the NLDAS environment through assimilation studies of soil moisture, snow, and terrestrial water storage, both serially and concurrently (e.g., Kumar et al. 2014, 2016, 2019a). Studies in other environments have also shown that data assimilation of remotely sensed products such as soil moisture can be beneficial toward monitoring agricultural drought (e.g., Yan and Moradkhani 2016; Ahmadalipour et al. 2017). These studies demonstrate that the assimilation of terrestrial hydrological datasets is helpful in not only improving the representation of water budget variables within LSMs, but also for improving the representation of extremes such as droughts.

One key limitation in many LDAS systems is that the LSMs often use climatologically based maps or look-up tables of vegetation states such as the green vegetation fraction (GVF) and/or the leaf area index (LAI). Through stomatal resistance, vegetation conditions on the land surface represent key controls on transpiration, evaporation, and the overall terrestrial water balance. LSMs within an LDAS that use climatological vegetation inputs will be fundamentally limited in representing interannual variations of the evapotranspiration and the land water and energy states (Ukkola et al. 2016). The LSMs will also be constrained in their ability to simulate rapidly emerging drought conditions, which feedback into vegetation growth and health (De Kauwe et al. 2015).

The Noah-MP LSM (Niu et al. 2011; Yang et al. 2011), which represents the next generation of the Noah LSM, contains several physics enhancements including: a multilayer snowpack, multiple options for runoff and infiltration, representation of an unconfined water table, and a dynamic vegetation scheme. The dynamic vegetation scheme adds biomass terms as prognostic variables, and the LAI is diagnosed from these masses, instead of input from maps or tables. Ma et al. (2017)

Corresponding author: David M. Mocko, david.mocko@nasa.gov

DOI: 10.1175/JHM-D-20-0065.1

used the dynamic vegetation scheme in Noah-MP with NLDAS Phase 2 (NLDAS-2) forcing, and found that the LSM was generally able to reproduce drought when compared to GRACE anomalies. However, Ma et al. (2017) also noted that Noah-MP was not able to accurately capture some recent droughts in areas with agricultural irrigation. Some previous studies have shown that improving the representation of vegetation in Noah-MP can lead to a better simulation in agricultural locations (e.g., Gayler et al. 2014; Poltoradnev et al. 2018).

Remotely sensed thermal-based evaporation estimates can be used to assess stress of the vegetation. One such product is the evaporative stress index (ESI; Anderson et al. 2007, 2011), calculated using anomalies of actual over potential evapotranspiration, using inputs of remotely sensed land surface temperature and LAI. Drought indices based on vegetation stress such as the ESI show skill in representing drought, particularly rapid onset drought (Otkin et al. 2013). Evaporative stress was shown to be a key feature of the 2012 ''flash drought'' in the central United States (Otkin et al. 2016; Basara et al. 2019). Vegetation and plant responses have been shown to be helpful for classifying and forecasting drought and vegetation conditions (e.g., Feng et al. 2018; Tian et al. 2019). Other drought indices based on vegetation stress include the Vegetation Drought Response Index (VegDRI; Brown et al. 2008) and the Quick Drought Response Index (QuickDRI; NDMC 2017).

With the development of prognostic vegetation within LSMs, there have been several efforts to introduce observational constraints through data assimilation of vegetation states such as LAI. These studies have demonstrated the positive impact of vegetation assimilation on evapotranspiration, root zone soil moisture, biomass, and CO_2 fluxes (e.g., Dente et al. 2008; Barbu et al. 2011; Ines et al. 2013; Albergel et al. 2017; Jin et al. 2018; Fox et al. 2018; Ling et al. 2019; Bonan et al. 2020). A few studies of vegetation assimilation have also examined their impact on drought estimation. Sabater et al. (2008), Barbu et al. (2014), and Sawada et al. (2020) all demonstrate that assimilation of LAI helps to provide a better representation of drought through improved representation of vegetation conditions.

In a recent effort (Kumar et al. 2019b), the impact of assimilating remote sensing-based LAI observations into the Noah-MP LSM was examined. A long-term climate data record of LAI from the University of Maryland's (UMD) Global Land Cover Facility (GLCF)—called the Global Land Surface Satellite (GLASS; Xiao et al. 2016)—was assimilated into the dynamic vegetation scheme of Noah-MP in the NLDAS environment. The study demonstrated systematic improvements in the terrestrial water and carbon budget terms due to LAI assimilation by comparing to a large suite of reference datasets. Overall, LAI assimilation had a beneficial impact on evapotranspiration, soil moisture, snow depth, terrestrial water storage, streamflow, and gross primary production (GPP). The most notable improvements were observed primarily over agricultural areas in the Midwest and Central Plains of the United States. This article extends the Kumar et al. (2019b) study by examining the impact of LAI assimilation on the LSM's ability to estimate agricultural drought.

The primary contribution of this study is the quantitative evaluation of the effects of LAI assimilation on model-estimated agricultural drought extent and severity against maps from a weekly operational drought monitor. The impact of LAI assimilation on drought characterization is examined by comparing drought categories from model simulations against drought monitor categories. Evaluations against in situ soil moisture observations as well as investigations of significant drought cases are also presented. Locations with human management of the landscape (such as irrigation) are examined to determine if LAI assimilation is helpful to the model's ability to characterize agricultural drought.

2. Approach

The NLDAS-2 (Xia et al. 2012) surface forcing is used to drive the Noah-MP (version 3.6) LSM over the continental United States, using a 1/8° latitude–longitude grid. The NASA-developed Land Information System (LIS; Kumar et al. 2006; Peters-Lidard et al. 2007) software framework is used to run the simulations. In this study, the prognostic vegetation capabilities in Noah-MP are utilized for incorporating observational constraints through data assimilation. The data assimilation integrations are conducted using a 1D ensemble Kalman filter (EnKF) algorithm.

The Kumar et al. (2019b) study used GLASS LAI values from MODIS, and focused their evaluation on an 18-yr period (2000–17). GLASS also provides LAI values from AVHRR starting from 1981, and a new data assimilation simulation is made using the GLASS AVHRR V4 data. The AVHRR-based simulations are used to provide a longer and consistent model climatology for this drought study. The GLASS AVHRR data are also available at 8-day intervals and on a 0.05° grid; a daily temporal interpolation is also performed. The MODIS-based LAI and AVHRR-based LAI fields are generally similar to each other, and comparable improvements to the water and carbon cycles are found from using AVHRR data (not shown) as from using MODIS. Kumar et al. (2019b) also provided figures showing differences in simulated top 1-m soil moisture, LAI, and other variables between simulations with and without LAI data assimilation, which are similar to results from using AVHRR data, so the reader is referred to their Fig. 2. As detailed in Kumar et al. (2019b), both the LAI observations and the modeled LAI are varied using additive perturbations with a standard deviation of 0.01. The ensemble generation also includes perturbations to the meteorological forcing inputs, with precipitation (P) and downward shortwave radiation (SW) having multiplicative perturbations with a mean of 1.0 and standard deviations of 0.3 (for P) and 0.5 (for SW), and the downward longwave radiation having additive perturbations with a standard deviation of $50\,\mathrm{W\,m^{-2}}$. The observation error standard deviation is set an optimistic level, which gives more weight to the LAI observations, and is comparable to values in previous studies (e.g., Albergel et al. 2017). Kumar et al. (2019b) showed that the seasonality of the LAI was improved over many cropland areas from this configuration of LAI DA.

Two separate simulations are performed. The first is an open-loop simulation (OL), with prognostic dynamic

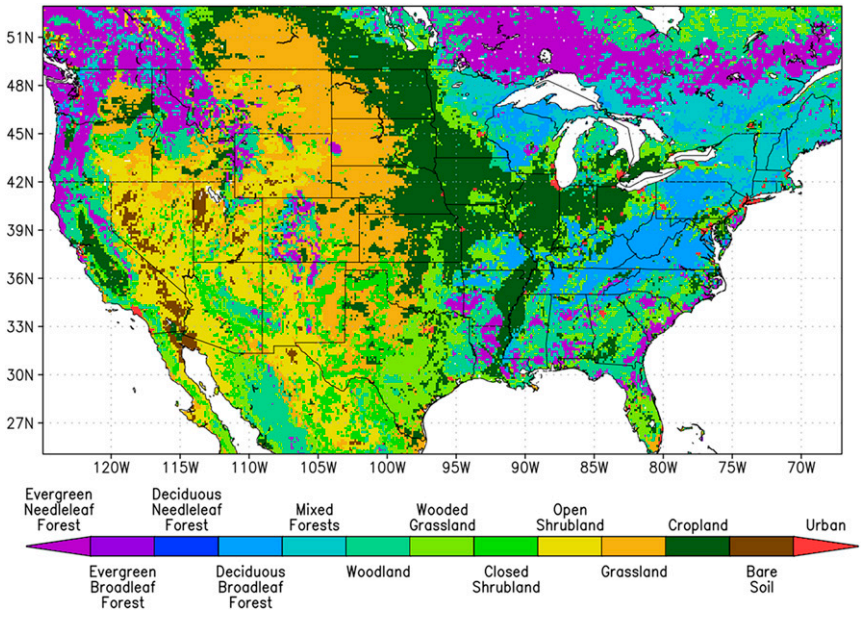

FIG. 1. Map of dominant land cover type using the UMD classification in the NLDAS domain.

vegetation, including the LAI, calculated by Noah-MP. The other simulation uses data assimilation (DA) of GLASS AVHRR to update the LAI in Noah-MP; the updated LAI is also used to update Noah-MP's leaf biomass consistent with the model's physics formulations. Only the LAI state in Noah-MP is updated directly from the GLASS AVHRR LAI observations. The land cover classification used in NLDAS is from UMD (Hansen et al. 2000), and a map of the domain and the land cover classification used in shown in Fig. 1.

As root zone soil moisture is often used as the basis for agricultural drought indicators (Bolten and Crow 2012), percentiles of the top 1-m soil moisture are used to develop estimates of drought. At each model grid cell, the climatology of top 1-m soil moisture is computed using the outputs from 39 years (January 1979–December 2017) of model simulations. Similar to the strategy used in the NLDAS drought monitor, a 5-day moving window is used to increase the sampling density in the daily climatology calculations (Kumar et al. 2014). The daily percentiles are then computed by ranking each day's top 1-m soil moisture against the empirical distribution obtained from the climatology at each grid cell. A separate model climatology is calculated for both the OL and the DA simulations. The NASA-developed Land Surface Verification Toolkit (LVT; Kumar et al. 2012) is used to perform the evaluations.

Consistent with the conventions used by the National Drought Mitigation Center (NDMC), five categories of drought intensity are defined as follows: D0 (abnormally dry, percentile $\leq 30\%$), D1 (moderate drought, percentile $\leq 20\%$), D2 (severe drought, percentile $\leq 10\%$), D3 (extreme drought, percentile $\leq 5\%$), and D4 (exceptional drought, percentile $\leq 2\%$). The weekly data archive from the U.S. Drought Monitor (USDM; Svoboda et al. 2002) of NDMC is used here for a quantitative evaluation of the drought estimates, with the drought categories from the USDM compared to the drought categories diagnosed from top 1-m soil moisture percentiles from both the OL and DA simulations to evaluate the effects of LAI assimilation.

The USDM is used here for intercomparison given the lack of other spatially and temporally complete drought data products. The USDM drought extent and severity map every week is produced by an author, who uses a "convergence of evidence approach" from various drought indicators as well as talking to local field experts. However, the USDM does have subjective roots, including from authors that rotate typically every couple of weeks, and has evolved over the years as more and finer-scale drought indicators have emerged over the decades. On the other hand, the drought categories from the model-simulated top 1-m soil moisture only represent agricultural drought, while the USDM will represent all droughts, including meteorological and hydrological as well. Comparisons to in situ soil moisture observations are presented to help provide confidence that using the USDM for assessing impacts on diagnosing agricultural drought is a reasonable approach.

3. Results

a. Comparison to in situ soil moisture

The simulated top 1-m soil moisture from both the OL and DA simulations are independently compared to in situ observations from the International Soil Moisture Network (ISMN; Dorigo et al. 2011). Comparisons are made at 934 stations from nine different observations networks within CONUS with observations at various levels to a depth of at least 1 m. The vertical average (weighted by soil layer thickness) for both

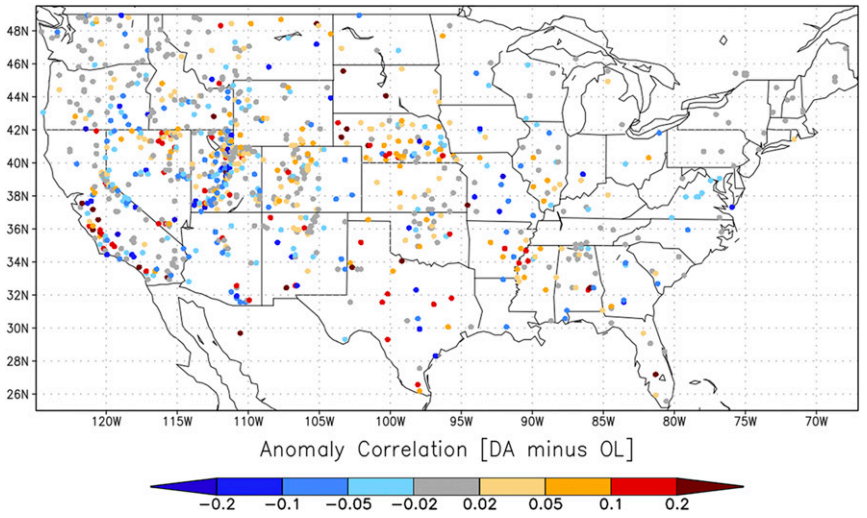

FIG. 2. Difference in the anomaly correlation of the top 1-m soil moisture as compared to ISMN in situ soil moisture observations for 18 years (2000–17), shown as the anomaly correlation of the DA run to the observations minus the anomaly correlation of the OL run to the observations. Warm colors (from orange to red) show areas there where is improved anomaly correlation of the simulated top 1-m soil moisture due to LAI assimilation.

the observations and the simulations is calculated, with data considered to be missing if not all profile measurements are available within the top 1 m. The anomaly correlation (AC), computed as the correlation of the differences between daily soil moisture values and their monthly mean, is calculated separately for the OL compared to the observations and for the DA compared to the observations.

Figure 2 shows the differences in the anomaly correlation, expressed as AC(DA versus ISMN) minus AC(OL versus ISMN) for the ISMN in situ observations. Positive values represent locations where the anomaly correlation of the top 1-m soil moisture improved compared to observations from LAI data assimilation. Areas with the greatest improvement include the central United States, the lower Mississippi, and parts of California. There are notable degradations in anomaly correlation over portions of the western United States and the Southeast. Many of the sites with improved top 1-m soil moisture simulation are

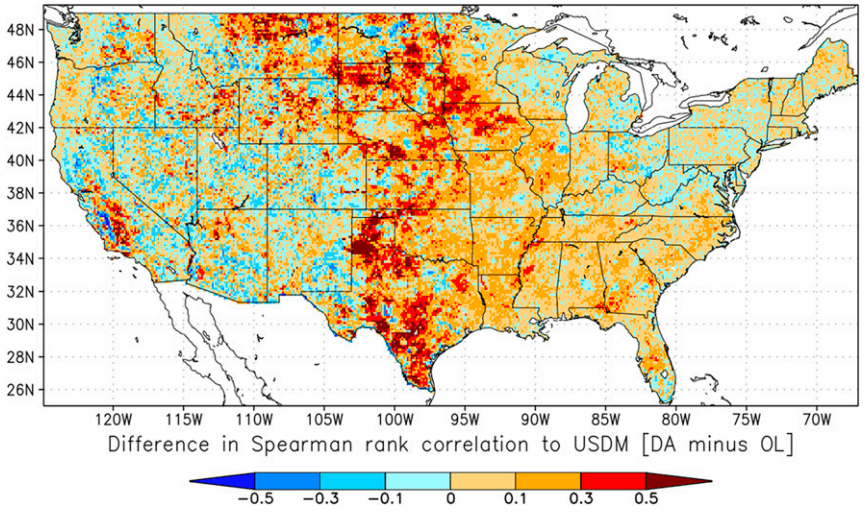

FIG. 3. Difference in the Spearman rank correlation of drought intensity estimates compared to the USDM data for 18 years (2000–17), shown as the correlation of the DA run to the USDM minus the correlation of the OL run to the USDM. For both model runs, percentiles of the top 1-m soil moisture are used to calculate the drought category. Warm colors (from orange to red) show areas where there is improved correlation to the USDM due to LAI assimilation.

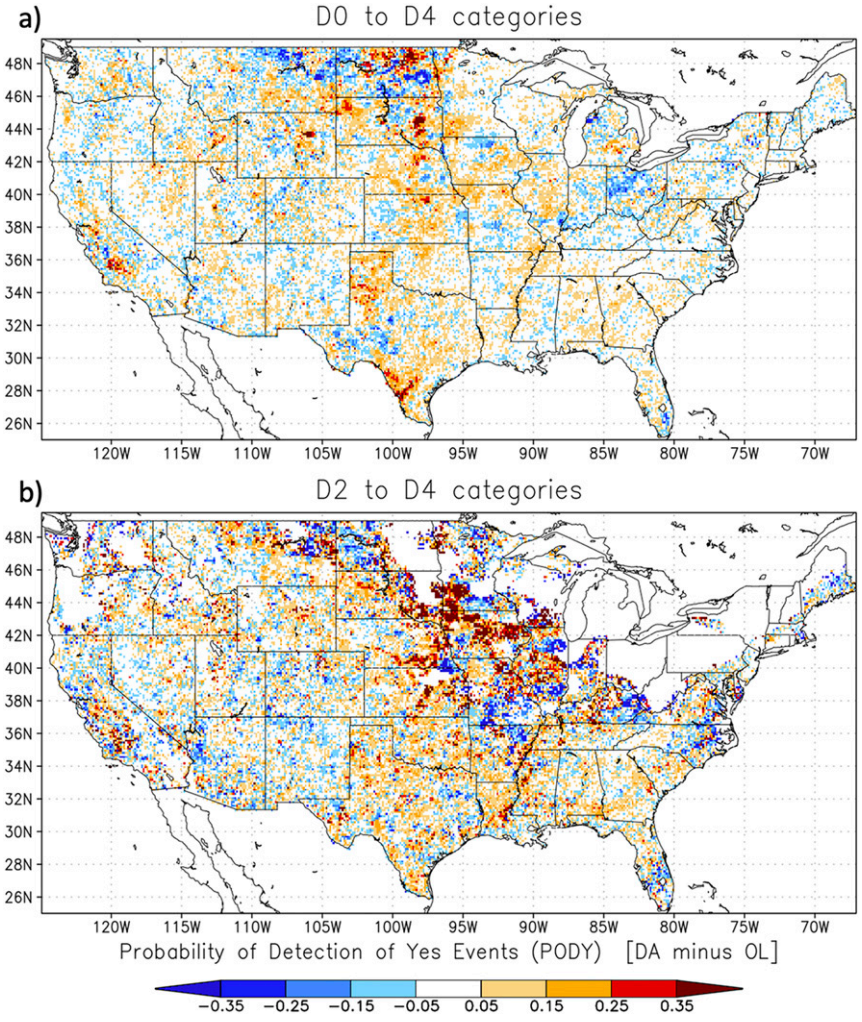

FIG. 4. Difference in probability of detection of "yes" events (PODY) compared to the USDM data for 18 years (2000–17), shown as the PODY of the DA run minus PODY of the OL run: (a) for all categories (D0–D4) and (b) for severe or worse drought categories (D2–D4). For both model runs, percentiles of the top 1-m soil moisture are used to calculate the drought category. Warm colors (from orange to red) show areas where the probability of drought detection has improved due to LAI assimilation.

identified as cropland in the UMD land cover classification shown in Fig. 1.

b. Comparison to the USDM

Figure 3 summarizes the beneficial impact of LAI assimilation on drought estimation. This figure shows the difference in the Spearman rank correlation (R) of the drought intensity categorization, calculated using percentiles of the top 1-m soil moisture as discussed above, using the weekly USDM maps as the reference. The rank correlation is used here as the correlations are calculated between the drought category from the USDM against the drought category determined from the top 1-m soil moisture percentiles. The correlations are computed during 2000–17, as the USDM archive starts in the year 2000. The figure is expressed as R(DA versus USDM) minus R(OL versus USDM), where the positive and negative values represent improvements and degradations in drought estimation due to the assimilation of LAI data, respectively. Figure 3 indicates that the impact of assimilation is generally positive, with significant improvements observed over the central United States, lower Mississippi basin, central valley of California, and the southeast United States. Comparatively, the impacts of assimilation over the Northeast and much of the western United States on drought are marginal. Note that many of the areas with the most improvement in correlation to the USDM are cropland in the UMD land cover classification. The more marginal improvements in cropland locations along and east of the Mississippi River are likely due to a combination of fewer drought events in the USDM, lower seasonality of monthly

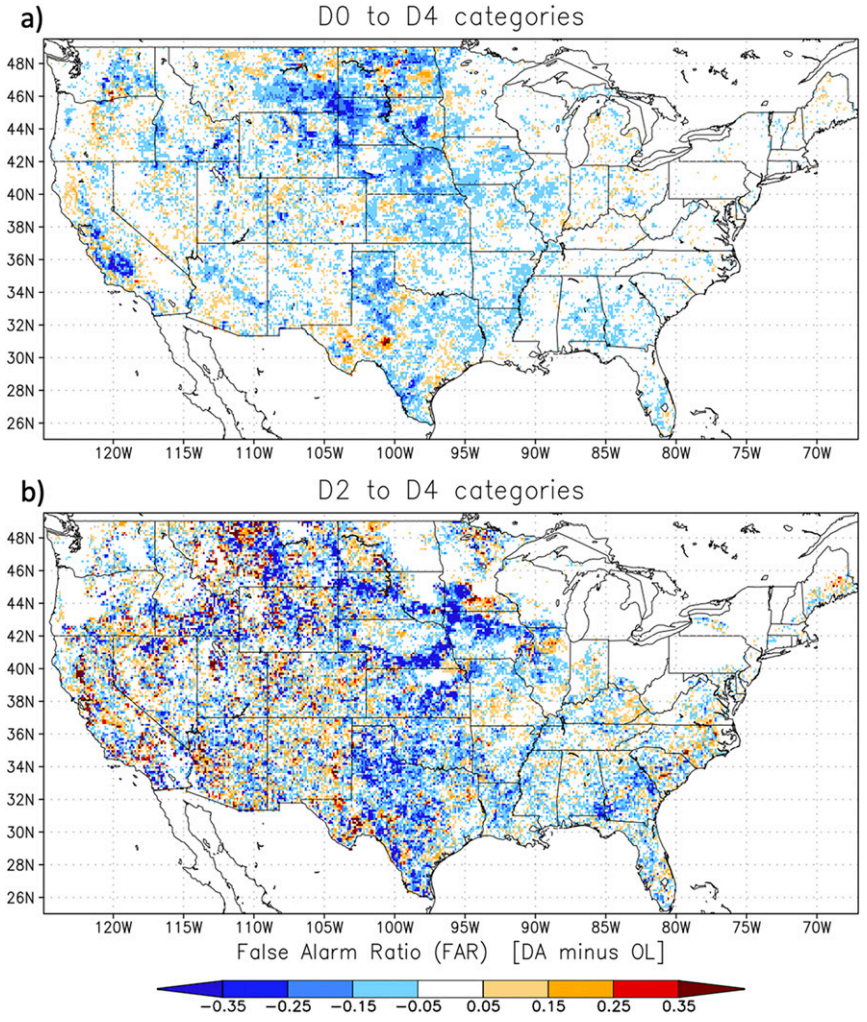

FIG. 5. Difference in false alarm ratio (FAR) compared to the USDM data for 18 years (2000–17), shown as the FAR of the DA run minus FAR of the OL run: (a) for all categories (D0–D4) and (b) for severe or worse drought categories (D2–D4). For both model runs, percentiles of the top 1-m soil moisture are used to calculate the drought category. Cold colors (blue) show areas where the drought false alarm ratio has reduced due to LAI assimilation.

precipitation, and higher summer LAI (in both OL and DA simulations) in these locations.

Figure 4 examines the ability of the simulations to detect drought events, again shown as a difference relative to the OL. The metric used is the probability of detection of ''yes'' events (PODY), which calculates the likelihood that the simulation will correctly diagnose drought events when they happen. The PODY is calculated as the number of ''hits,'' or correctly simulated drought events, over the sum of the hits and ''misses,'' or drought events shown in the USDM but not simulated by the LSM. Figure 4 shows the PODY for the DA simulation minus the PODY for the OL. Figure 4a shows the difference for all drought categories (D0–D4), while Fig. 4b shows the difference for only severe or worse drought (D2–D4). For the D0–D4 to be considered a hit, both the USDM and the model must be at least D0; similarly, for the D2–D4 to be a hit, both the USDM and the model must be at least D2. The positive values indicate areas where LAI data assimilation improves the model's ability to detect drought. Areas with the most improvements are in similar locations as shown in Fig. 3. Notably, some areas show a stronger improvement for severe or worse droughts (Fig. 4b) than for all drought categories (Fig 4a); this demonstrates that LAI DA can be particularly helpful with severe drought detection. Further investigation revealed that both the OL and DA simulations tended to capture at least a representation of mild dry or drought conditions due to them both using the same precipitation forcing. By definition, there are fewer severe or worse droughts than all droughts, and the OL was not able to detect several of these severe droughts, while the DA was to do so.

Figure 5 is similar to Fig. 4, except it shows the difference in the false alarm ratio (FAR). ''False alarms'' are when the model simulated a drought, which was not shown in the

TABLE 1. Stratification of changes in drought metrics (DA minus OL) by UMD land cover classification as well as by irrigated area as determined by NCA-LDAS. The cropland land cover class is bold to highlight the greatest improvement in the metrics among the UMD land cover classes.

UMD land cover class	Percent area in CONUS (%)	Rank R	PODY (D0–D4)	PODY (D2–D4)	FAR (D0–D4)	FAR (D2–D4)
Evergreen needleleaf forest	7.6	0.026	0.005	0.015	−0.006	−0.011
Deciduous broadleaf forest	8.1	0.022	0.002	0.001	−0.005	0.0
Mixed forests	5.6	0.026	0.005	0.003	−0.006	−0.002
Woodland	12.1	0.034	0.003	0.009	−0.008	−0.015
Wooded grassland	13.0	0.100	0.022	0.036	−0.023	−0.031
Closed shrubland	3.9	0.108	0.018	0.032	−0.031	−0.048
Open shrubland	10.5	0.032	0.012	0.013	−0.016	−0.015
Grassland	17.7	0.112	0.015	0.026	−0.042	−0.037
Cropland	**19.3**	**0.153**	**0.037**	**0.089**	**−0.045**	**−0.059**
Irrigated areas	14.6	0.153	0.035	0.047	−0.055	−0.061
Nonirrigated areas	85.4	0.067	0.013	0.029	−0.019	−0.023

USDM. The FAR is calculated as the false alarms over the sum of hits plus false alarms. The negative values are locations where LAI data assimilation reduced the number of false alarms, thus improving model behavior to only simulate drought when it is diagnosed to occur. Again, areas with the most improvement are the cropland areas, and the FAR improvement is often greater for severe or worse droughts.

Table 1 stratifies the results for each of these metrics for the UMD land cover classes. Only UMD land cover classes with more than 3% areal coverage in CONUS are shown. For forest classes (the first four rows), the average increase in correlation and PODY is positive but small. The average decrease in FAR is also small and negative, indicating that LAI data assimilation has a small but beneficial benefit in the ability of the model to depict drought in forested areas. The next four rows are for grassland and shrubland land classes. The correlation differences are generally higher than for the forest classes, with corresponding improvements in the PODY and FAR. The cropland class is shown to have the highest increase in correlation to the USDM as well as the highest increase in PODY

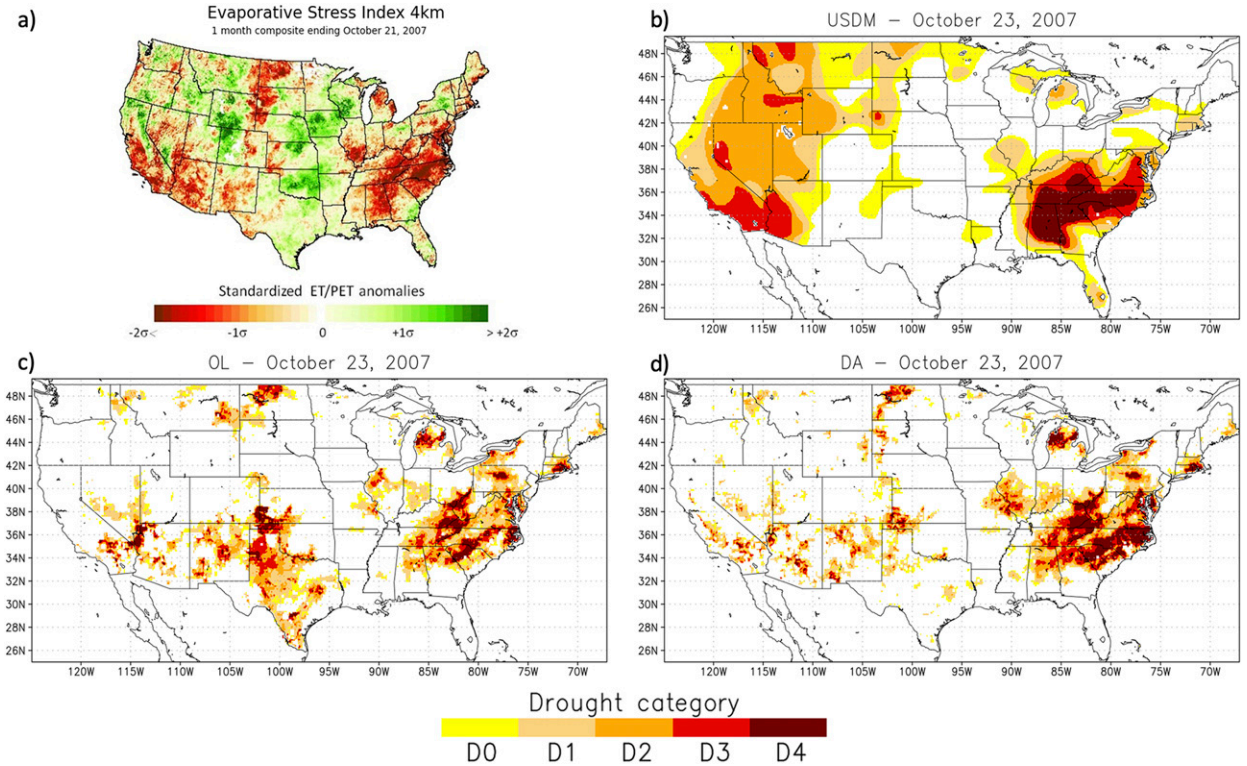

FIG. 6. Drought depiction for the third week of October 2007: (a) the ESI for 21 Oct 2007; (b) USDM categories for 23 Oct 2007; (c) OL categories, from percentiles of the top 1-m soil moisture, also for 23 Oct 2007; and (d) as in (c), but for the DA run.

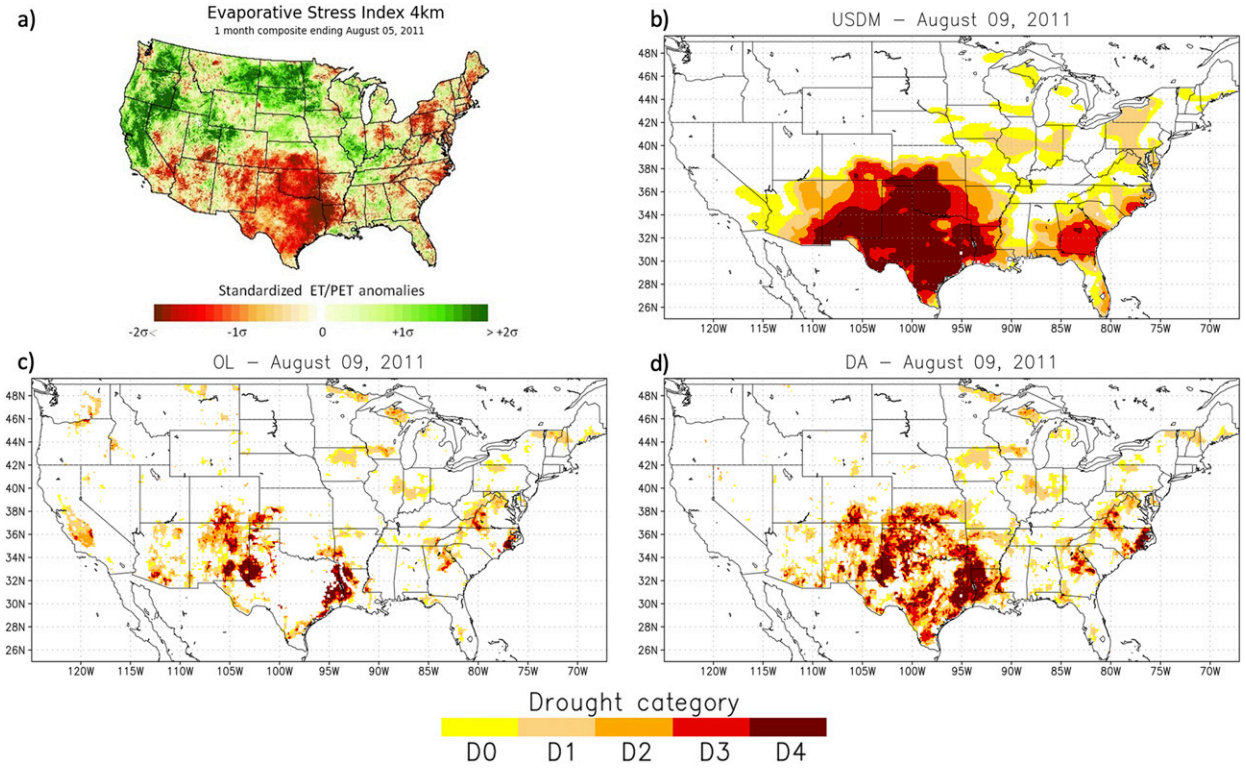

FIG. 7. As in Fig. 6, but for early August 2011: (a) the ESI for 5 Aug 2011; (b)–(d) USDM, OL, and DA, respectively, for 9 Aug 2011.

(>3%); the increase is substantially higher (>8%) when considering only severe or worse droughts. Also shown on Table 1 are metrics when stratified by irrigated area. Irrigated area is determined from the National Climate Assessment–LDAS (NCA-LDAS; Kumar et al. 2019a; Jasinski et al. 2019) using a demand-driven approach using a MODIS classification scheme (Ozdogan et al. 2010); only areas with at least an average of 10 mm yr^{-1} are considered to be irrigated for this stratification. It is important to note that no irrigation occurs in either the OL or DA simulation in this study. The areas likely to be undergoing irrigation have a higher increase in correlation to the USDM as well as a higher PODY and a greater decrease in FAR. This analysis indicates that despite no irrigation occurring in these simulations, LAI data assimilation is able to improve the model's ability to depict agricultural drought by incorporating more realistic vegetation states, which is bolstered by the improvement to simulated soil moisture in these locations as previously discussed.

c. *Drought cases*

Several severe drought cases are examined in detail to demonstrate changes in the drought percentiles from LAI data assimilation as compared to the USDM. Maps of the ESI are also compared, to show areas undergoing vegetation stress. The first case is from 23 October 2007 and is shown in Fig. 6. The USDM shows exceptional drought in the southeast United States, which is underestimated by the OL. The OL also overestimates drought over Texas significantly. The DA run improves both these representations, producing a stronger drought than OL over the southeast and removing the spurious drought estimates over Texas. The ESI map for the same week also shows the extreme drought in the southeast, with little vegetation stress in Texas.

The second case is a drought in Texas in 2011 (Fig. 7). The USDM map for 9 August 2011 shows an exceptional drought over nearly all of Texas. The OL run poorly represents this drought in Texas. The DA run improves the drought characterization, though it is still underestimated in a few locations relative to the USDM map on this date. However, the ESI map for this week also shows relatively weaker vegetation stress in many of the same locations where the DA run also has a weaker drought than the USDM. In central California, the OL estimates a moderate drought that is not shown in the USDM; the DA simulation no longer shows a drought here. This is an example of a false alarm in the OL, demonstrating that LAI DA correctly simulates no drought in California during this week.

Figure 8 shows maps from the flash drought event of 2012 in the central United States. A widespread extreme drought is shown over a wide area. The OL run simulates many areas with no drought categories. The DA run does a significantly better job in simulating this drought, particularly over eastern Nebraska, Iowa, Missouri, and Illinois, as compared to both the USDM and the ESI. Most of these areas are identified as cropland in the UMD land cover classification.

Figure 9 shows an area-average time series of the behavior of the Noah-MP dynamic vegetation OL and DA simulations for the 2012 drought for an area over eastern Nebraska and

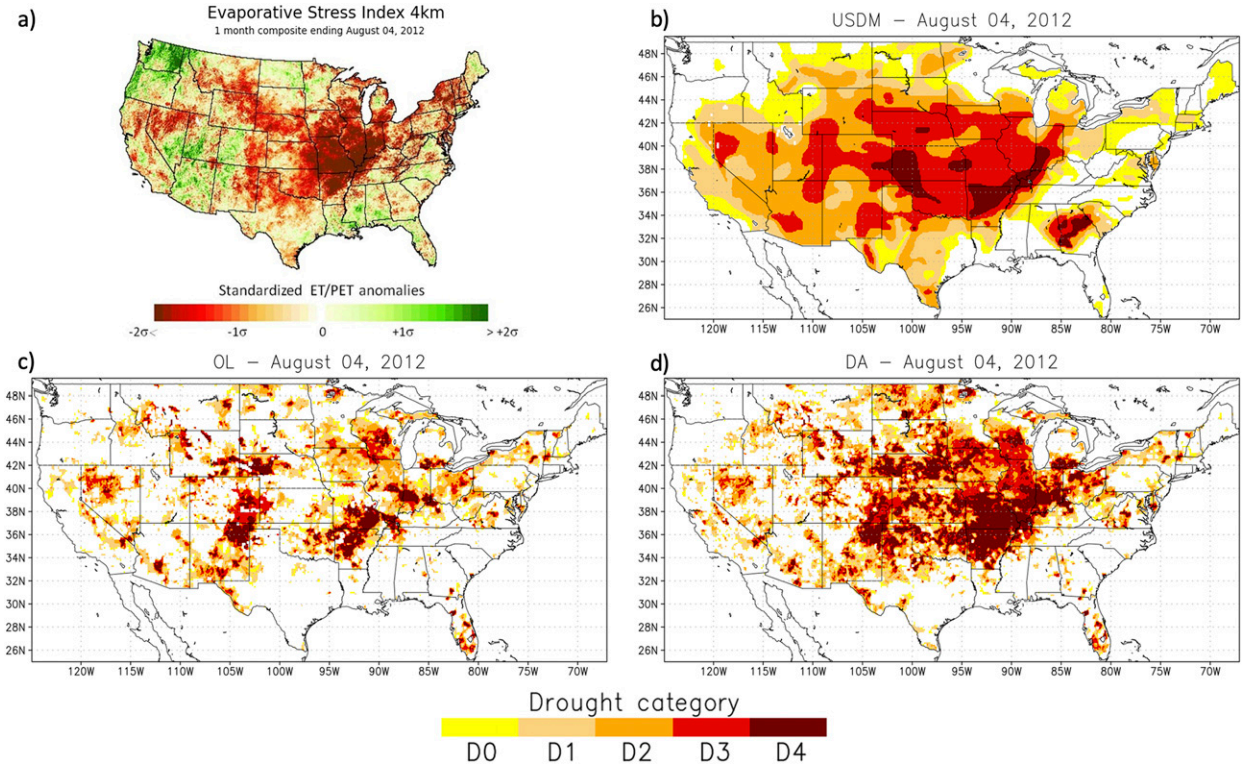

FIG. 8. As in Fig. 6, but for early August 2012: (a) the ESI for 4 Aug 2012; (b)–(d) USDM, OL, and DA, respectively, for 4 Aug 2012.

western Iowa. This area (shown as the inset of Fig. 9b) is dominated by the cropland class in the UMD classification, and also has a significant portion of the area likely to be irrigated. The OL prognostic LAI increases quickly during the spring, peaking in early June. When DA is performed, the LAI is lower than the OL in the spring, but continues to increase later into the summer. Thus, LAI DA corrects the seasonality of the vegetation. The lower LAI in the OL later in the summer produces lower total evapotranspiration (not shown), which results in a top 1-m soil moisture that remains relatively wet. When DA is performed, the summer LAI is higher than in the OL. The higher LAI results in additional transpiration, which removes the top 1-m soil moisture. The lower soil moisture leads to the diagnosis of more severe drought categories during the summer of 2012 from the soil moisture percentiles. The residual zig-zag pattern in the DA simulation's LAI is from model drift of other prognostic variables not updated through data assimilation (such as the wood, stem, and root masses in the dynamic vegetation scheme) as well as from the bookends changing from the daily interpolation of the 8-day LAI observations.

Figure 10 shows an area-average time series for the state of Texas (shown as the inset of Fig. 10b) during 2007. In this case, the OL incorrectly diagnoses a drought that was not shown in the USDM maps. For most of the year, the OL LAI is higher than the LAI from the DA simulation. This results in the soil moisture being slightly drier in the OL as compared to the DA, corresponding to some diagnosis of drought areas in the OL shown in Fig. 6. The DA simulation corrects this overestimation of drought by improving the simulation of the LAI during the year.

In many agricultural locations, the dynamic vegetation scheme in Noah-MP is often unable to accurately represent the actual vegetation and LAI. During drought periods, the surface soil moisture becomes dry due to the lack of precipitation, which in turn lowers the model's leaf vegetation mass, lowering the LAI. However, the root zone soil moisture does not get depleted as the low LAI leads to reduced transpiration through the vegetation. The surface bare soil evaporation does not increase enough to dry the soil to represent an agricultural drought through the root zone. With data assimilation, the underestimation in LAI is corrected, leading to increased transpiration and reduced root zone soil moisture. Similarly, a reduction in the LAI from LAI DA can lead to reduced transpiration and increased root zone soil moisture, which subsequently enables the correction of overestimated drought intensities (in cases such as the 23 October 2007 example in Texas).

4. Summary and discussion

This study presents an evaluation of a land surface model (LSM) simulation of agricultural drought both with and without assimilation of leaf area index (LAI) observations. The Noah-MP LSM is used in the NLDAS-2 environment, and GLASS AVHRR LAI is assimilated into the dynamic vegetation scheme of Noah-MP. Drought categories diagnosed from simulated top 1-m soil moisture percentiles (representing

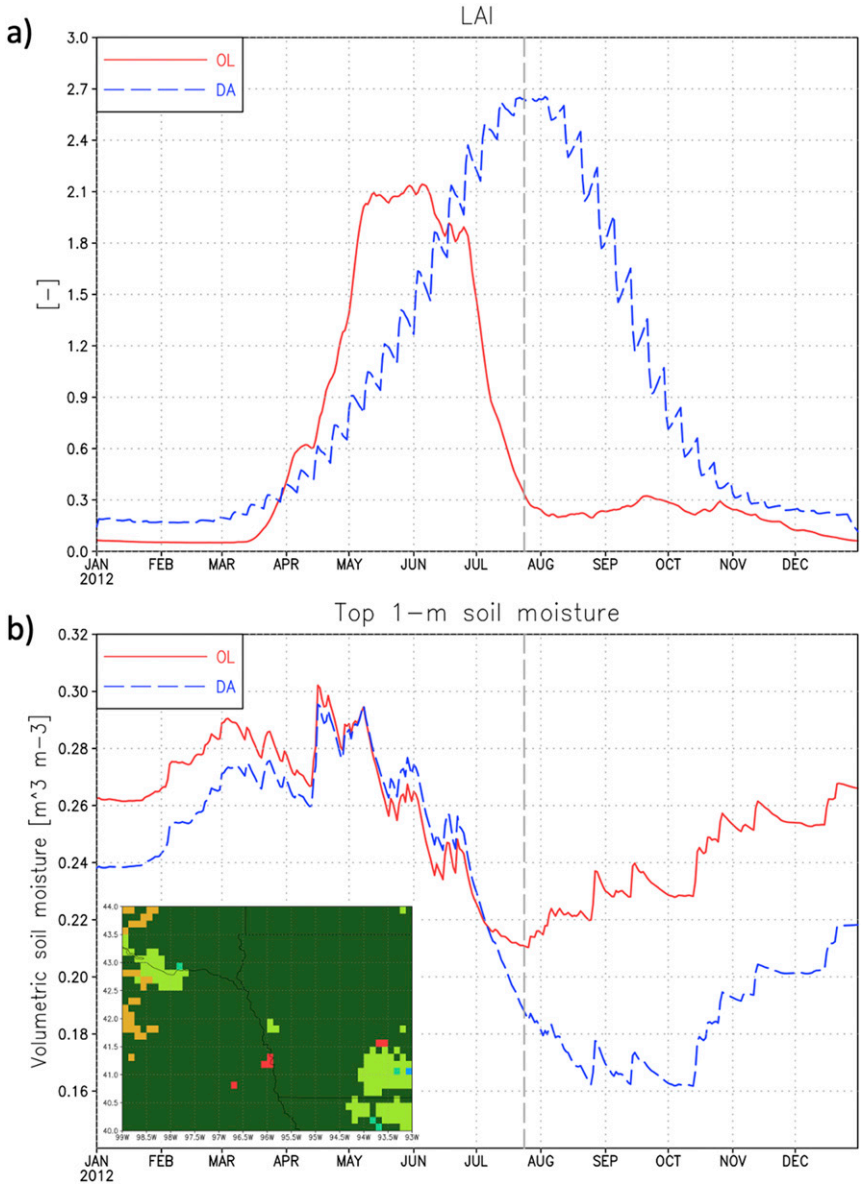

FIG. 9. Area-averaged time series for a box between 99° and 93°W and between 40° and 44°N (eastern Nebraska and western Iowa) during 2012 of (a) LAI and (b) top 1-m soil moisture. The red solid curve is for the OL run; the blue dashed curve is for the DA run. The thick vertical gray dashed line on 24 Jul 2012 indicates when the USDM first had more than 50% of this area in D2 or worse drought during this event. The area included in the area-average of the box is shown as the inset in (b), using the UMD land cover classification colors from Fig. 1.

agricultural drought) are compared to weekly drought categories from U.S. Drought Monitor maps from 2000 to 2017. Correlation, probability of detection, and false alarm ratio are the metrics used for the drought evaluation. The quantitative evaluation of changes to model-simulated agricultural drought extent and severity from vegetation assimilation is a distinguishing feature of this study.

The assimilation of LAI observations into Noah-MP generally improves drought extent and intensity estimations. The most notable improvements to simulated drought are shown in agricultural locations likely to be undergoing irrigation. This improvement is found despite the fact that no irrigation was simulated in this study. The LAI assimilation in observed drought periods in these locations tends to increase the LAI over the simulation without assimilation. The higher LAI produces more transpiration and a lower simulated soil moisture through the root zone, better simulating the agricultural drought. It is noted that the LAI data assimilation tends to have a greater improvement in correlation, probability of detection, and false alarms, for more severe droughts,

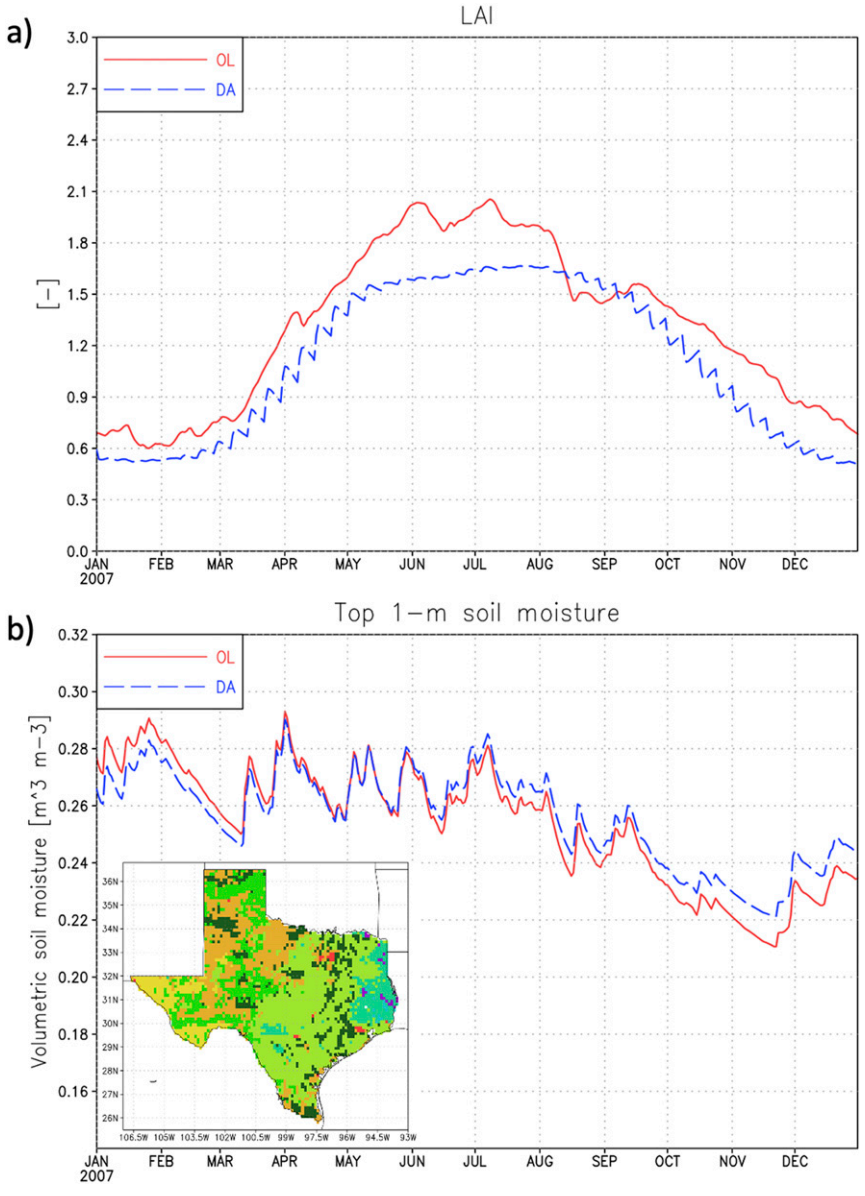

FIG. 10. Area-averaged time series for the state of Texas during 2007 of (a) LAI and (b) top 1-m soil moisture. The red solid curve is for the OL run; the blue dashed curve is for the DA run. The area included in the area-average for the state of Texas is shown as the inset in (b), using the UMD land cover classification colors from Fig. 1.

indicating that the proper representation of vegetation conditions within a LSM is crucial for these extreme events.

The dynamic vegetation scheme of Noah-MP generally performs well in its response to meteorological drought (precipitation deficit) over many locations. However, the model often does not represent agricultural drought in areas likely to be undergoing irrigation. The assimilation of LAI into the dynamic vegetation scheme thus does not merely correct errors in Noah-MP's simulation of leaf mass and other vegetation masses; it helps the model compensate its inability to represent unmodeled processes, such as irrigation. Assimilation of surface soil moisture retrievals in irrigated areas previously showed limited skill toward improving simulated surface soil moisture (Kumar et al. 2015). For simulating root zone soil moisture and representing agricultural drought, the assimilation of LAI supports more accurate transpiration resulting in an improved drought estimation over multiple land-cover types, but especially over agricultural locations.

The robustness of these results should be tempered by the subjective and evolving nature of the USDM weekly maps. Since the start of the evaluation period in 2000 to the end in 2017, the USDM authors have had access to a growing and

ever-improving (in both quality and spatial scale) drought indicators, which has resulted in changes to the smoothness and scale of the boundaries between drought categories. The evaluations that were performed are comparing these changing maps to model data on the 1/8° NLDAS grid over the 18-yr period. The weekly USDM maps are adjusted with input from local experts, and individual authors may emphasize different products/inputs when drawing their weekly maps—both of which are difficult to reproduce in a model environment. Additionally, by definition the model percentiles are calculated over their 39-yr simulation period, while the USDM maps are drawn each week using a convergence of evidence approach from the products available that week. Finally, there were more dry and severe drought conditions over the west and central United States than in the east over the 18-yr evaluation period, in both the USDM and the model simulations. Still, given the consistent improvement in correlation, probability of detection, and false alarm ratio in cropland and areas likely to be irrigated, the assimilation of LAI is shown to improve drought estimation as compared to the USDM.

In addition to LAI data assimilation, there are other active areas of development to improve an LSM's ability to simulate drought, including both model physics and assimilating other products. For example, Niu et al. (2020) have added a representation of plant water storage from root water uptake in Noah-MP, and found an improved response to drought. Several recent works have examined the effects of simultaneous assimilation of soil moisture and LAI (e.g., Sabater et al. 2008; Ines et al. 2013; Barbu et al. 2014; Albergel et al. 2017). The focus of this study, however, is purely on LAI assimilation, and identifying locations where LAI DA is beneficial to representing drought. Vegetation optical depth (VOD), retrieved using microwave radiometers, has been shown to a proxy for vegetation states such as biomass and vegetation water stress (Liu et al. 2019). VOD also provides an all-weather capability for vegetation remote sensing, unlike optical products such as the LAI. Recent work by Kumar et al. (2020) has found that VOD assimilation in the Noah-MP LSM also improves the simulation of evapotranspiration, particularly over agricultural areas. Future work will also explore the assimilation of thermal-based retrievals, such as the ESI, into Noah-MP. The expectation is that these enhancements will potentially improve the model's ability to simulate water states and drought in areas under human water management, such as irrigation.

Acknowledgments. This study was supported by NOAA's Climate Program Office's Modeling, Analysis, Predictions, and Projections (MAPP) program (Grant GC17-701A). Dr. Peters-Lidard served as the Lead of the NOAA MAPP Drought Task Force III, with Mr. Mocko and Dr. Kumar also participating in the Drought Task Force. Computing was supported by the resources at the NASA Center for Climate Simulation. The NLDAS-2 forcing data used in this effort were acquired as part of the activities of NASA's Science Mission Directorate, and are archived and distributed by the Goddard Earth Sciences (GES) Data and Information Services Center (DISC). The University of Maryland's Global Land Cover Facility (GLCF) and Beijing Normal University are thanked for their efforts with the GLASS LAI. The ESI maps were obtained from the USDA-ARS HRSL image archive. Three anonymous reviewers and the editor are thanked for their comments and suggestions in improving this manuscript.

REFERENCES

Ahmadalipour, A., H. Moradkhani, H. Yan, and M. Zarekarizi, 2017: Remote sensing of drought: Vegetation, soil moisture, and data assimilation. *Remote Sensing of Hydrological Extremes*, V. Lakshmi, Ed., Springer, 121–149, https://doi.org/10.1007/978-3-319-43744-6_7.

Albergel, C., and Coauthors, 2017: Sequential assimilation of satellite-derived vegetation and soil moisture products using SURFEX_v8.0: LDAS-monde assessment over the Euro-Mediterranean area. *Geosci. Model Dev.*, **10**, 3889–3912, https://doi.org/10.5194/gmd-10-3889-2017.

Anderson, M. C., J. M. Norman, J. R. Mecikalski, J. A. Otkin, and W. P. Kustas, 2007: A climatological study of evapotranspiration and moisture stress across the continental United States based on thermal remote sensing: 2. Surface moisture climatology. *J. Geophys. Res.*, **112**, D11112, https://doi.org/10.1029/2006JD007507.

——, C. Hain, B. Wardlow, A. Pimstein, J. R. Mecikalski, and W. P. Kustas, 2011: Evaluation of drought indices based on thermal remote sensing of evapotranspiration over the continental United States. *J. Climate*, **24**, 2025–2044, https://doi.org/10.1175/2010JCLI3812.1.

Barbu, A. L., J.-C. Calvet, J.-F. Mahfouf, C. Albergel, and S. Lafont, 2011: Assimilation of soil wetness index and leaf area index into the ISBA-A-gs land surface model: Grassland case study. *Biogeosciences*, **8**, 1971–1986, https://doi.org/10.5194/bg-8-1971-2011.

——, ——, ——, and S. Lafont, 2014: Integrating ASCAT surface soil moisture and GEOV1 leaf area index into the SURFEX modelling platform: A land data assimilation application over France. *Hydrol. Earth Syst. Sci.*, **18**, 173–192, https://doi.org/10.5194/hess-18-173-2014.

Basara, J. B., J. I. Christian, R. A. Wakefield, J. A. Otkin, E. D. Hunt, and D. P. Brown, 2019: The evolution, propagation, and spread of flash drought in the central United States during 2012. *Environ. Res. Lett.*, **14**, 084025, https://doi.org/10.1088/1748-9326/ab2cc0.

Bolten, J. D., and W. T. Crow, 2012: Improved prediction of quasi-global vegetation conditions using remotely-sensed surface soil moisture. *Geophys. Res. Lett.*, **39**, L19406, https://doi.org/10.1029/2012GL053470.

Bonan, B., C. Albergel, Y. Zheng, A. L. Barbu, D. Fairbairn, S. Munier, and J.-C. Calvet, 2020: An ensemble square root filter for the joint assimilation of surface soil moisture and leaf area index within the land data assimilation system LDAS-Monde: Application over the Euro-Mediterranean region. *Hydrol. Earth Syst. Sci.*, **24**, 325–347, https://doi.org/10.5194/hess-24-325-2020.

Brown, J. F., B. D. Wardlow, T. Tadesse, M. J. Hayes, and B. C. Reed, 2008: The Vegetation Drought Response Index (VegDRI): A new integrated approach for monitoring drought stress in vegetation. *GIsci. Remote Sens.*, **45**, 16–46, https://doi.org/10.2747/1548-1603.45.1.16.

De Kauwe, M. G., S.-X. Zhou, B. E. Medlyn, A. J. Pitman, Y.-P. Wang, R. A. Duursma, and I. C. Prentice, 2015: Do land surface models need to include differential plant species responses to drought? Examining model predictions across a mesic-xeric gradient in Europe. *Biogeosciences*, **12**, 7503–7518, https://doi.org/10.5194/bg-12-7503-2015.

Dente, L., G. Satalino, F. Mattia, and F. Rinaldi, 2008: Assimilation of Leaf Area Index derived from ASAR and MERIS data into CERES-Wheat model to map wheat yield. *Remote Sens. Environ.*, **112**, 1395–1407, https://doi.org/10.1016/j.rse.2007.05.023.

Dorigo, W., P. van Oevelen, W. Wagner, S. Mecklenburg, A. Robock, and T. Jackson, 2011: A new international network for soil moisture data. *Eos, Trans. Amer. Geophys. Union*, **92**, 141–142, https://doi.org/10.1029/2011EO170001.

Ek, M. B., and Coauthors, 2011: North American Land Data Assimilation System Phase 2 (NLDAS-2): Development and applications. *GEWEX News*, Vol. 21, No. 2, International GEWEX Project Office, Silver Spring, MD, 6–7, https://www.gewex.org/gewex-content/files_mf/1432209506May2011.pdf.

Feng, X., D. D. Ackerly, T. E. Dawson, S. Manzoni, R. P. Skelton, G. Vico, and S. E. Thompson, 2018: The ecohydrological context of drought and classification of plant responses. *Ecol. Lett.*, **21**, 1723–1736, https://doi.org/10.1111/ele.13139.

Fox, A. M., and Coauthors, 2018: Evaluation of a data assimilation system for land surface models using CLM4.5. *J. Adv. Model. Earth Syst.*, **10**, 2471–2494, https://doi.org/10.1029/2018MS001362.

Gayler, S., and Coauthors, 2014: Incorporating dynamic root growth enhances the performance of Noah-MP at two contrasting winter wheat field sites. *Water Resour. Res.*, **50**, 1337–1356, https://doi.org/10.1002/2013WR014634.

Hansen, M. C., R. S. DeFries, J. R. G. Townshend, and R. Sohlberg, 2000: Global land cover classification at 1km spatial resolution using a classification tree approach. *Int. J. Remote Sens.*, **21**, 1331–1364, https://doi.org/10.1080/014311600210209.

Hao, Z., A. AghaKouchak, N. Nakhjiri, and A. Farahmand, 2014: Global integrated drought monitoring and prediction system. *Sci. Data*, **1**, 140001, https://doi.org/10.1038/sdata.2014.1.

Houborg, R., M. Rodell, B. Li, R. Reichle, and B. F. Zaitchik, 2012: Drought indicators based on model-assimilated Gravity Recovery and Climate Experiment (GRACE) terrestrial water storage observations. *Water Resour. Res.*, **48**, W07525, https://doi.org/10.1029/2011WR011291.

Ines, A. V. M., N. N. Das, J. W. Hansen, and E. G. Njoku, 2013: Assimilation of remotely sensed soil moisture and vegetation with a crop simulation model for maize yield prediction. *Remote Sens. Environ.*, **138**, 149–164, https://doi.org/10.1016/j.rse.2013.07.018.

Jasinski, M. F., and Coauthors, 2019: NCA-LDAS: Overview and analysis of hydrologic trends for the National Climate Assessment. *J. Hydrometeor.*, **20**, 1595–1617, https://doi.org/10.1175/JHM-D-17-0234.1.

Jin, X., L. Kumar, Z. Li, H. Feng, X. Xu, G. Yang, and J. Wang, 2018: A review of data assimilation of remote sensing and crop models. *Eur. J. Agron.*, **92**, 141–152, https://doi.org/10.1016/j.eja.2017.11.002.

Kumar, S. V., and Coauthors, 2006: Land Information System: An interoperable framework for high resolution land surface modeling. *Environ. Modell. Software*, **21**, 1402–1415, https://doi.org/10.1016/j.envsoft.2005.07.004.

——, C. D. Peters-Lidard, J. Santanello, K. Harrison, Y. Liu, and M. Shaw, 2012: Land surface Verification Toolkit (LVT) - A generalized framework for land surface model evaluation. *Geosci. Model Dev.*, **5**, 869–886, https://doi.org/10.5194/gmd-5-869-2012.

——, and Coauthors, 2014: Assimilation of remotely sensed soil moisture and snow depth retrievals for drought estimation. *J. Hydrometeor.*, **15**, 2446–2469, https://doi.org/10.1175/JHM-D-13-0132.1.

——, C. D. Peters-Lidard, J. A. Santanello, R. H. Reichle, C. S. Draper, R. D. Koster, G. Nearing, and M. F. Jasinski, 2015: Evaluating the utility of satellite soil moisture retrievals over irrigated areas and the ability of land data assimilation methods to correct for unmodeled processes. *Hydrol. Earth Syst. Sci.*, **19**, 4463–4478, https://doi.org/10.5194/hess-19-4463-2015.

——, and Coauthors, 2016: Assimilation of gridded GRACE terrestrial water storage estimates in the North American Land Data Assimilation System. *J. Hydrometeor.*, **17**, 1951–1972, https://doi.org/10.1175/JHM-D-15-0157.1.

——, M. J. Jasinski, D. M. Mocko, M. Rodell, J. Borak, B. Li, H. Kato Beaudoing, and C. D. Peters-Lidard, 2019a: NCA-LDAS land analysis: Development and performance of a multisensor, multivariate land data assimilation system for the National Climate Assessment. *J. Hydrometeor.*, **20**, 1571–1593, https://doi.org/10.1175/JHM-D-17-0125.1.

——, D. M. Mocko, S. Wang, and C. D. Peters-Lidard, 2019b: Assimilation of remotely sensed leaf area index into the Noah-MP land surface model: Impacts on water and carbon fluxes and states over the continental United States. *J. Hydrometeor.*, **20**, 1359–1377, https://doi.org/10.1175/JHM-D-18-0237.1.

——, T. R. Holmes, R. Bindlish, R. de Jeu, and C. D. Peters-Lidard, 2020: Assimilation of vegetation optical depth retrievals from passive microwave radiometry. *Hydrol. Earth Syst. Sci.*, **24**, 3431–3450, https://doi.org/10.5194/hess-24-3431-2020.

Ling, X.-L., C.-B. Fu, Z.-L. Yang, and W.-D. Guo, 2019: Comparison of different sequential assimilation algorithms for satellite-derived leaf area index using the Data Assimilation Research Testbed (version Lanai). *Geosci. Model Dev.*, **12**, 3119–3133, https://doi.org/10.5194/gmd-12-3119-2019.

Liu, R., J. Wen, X. Wang, Z. Wang, Z. Li, Y. Xie, L. Zhu, and D. Li, 2019: Derivation of vegetation optical depth and water content in the source region of the Yellow River using the FY-3B microwave data. *Remote Sens.*, **11**, 1536, https://doi.org/10.3390/rs11131536.

Ma, N., G.-Y. Niu, Y. Xia, X. Cai, Y. Zhang, Y. Ma, and Y. Fang, 2017: A systematic evaluation of Noah-MP in simulating land-atmosphere energy, water, and carbon exchanges over the continental United States. *J. Geophys. Res. Atmos.*, **122**, 12 245–12 268, https://doi.org/10.1002/2017JD027597.

Mo, K. C., L. N. Long, Y. Xia, S. K. Yang, J. E. Schemm, and M. Ek, 2011: Drought indices based on the Climate Forecast System Reanalysis and ensemble NLDAS. *J. Hydrometeor.*, **12**, 181–205, https://doi.org/10.1175/2010JHM1310.1.

NDMC, 2017: Quick drought response index: A short-term dryness indicator. National Drought Mitigation Center Publ. 9, 3 pp., https://digitalcommons.unl.edu/ndmcpub/9/.

Niu, G.-Y., and Coauthors, 2011: The community Noah land surface model with multiparameterization options (Noah-MP): 1. Model description and evaluation with local-scale measurements. *J. Geophys. Res.*, **116**, D12109, https://doi.org/10.1029/2010JD015139.

——, Y.-H. Fang, L.-L. Chang, J. Jin, H. Yuan, and X. Zeng, 2020: Enhancing the Noah-MP's ecosystem response to droughts with an explicit representation of plant water storage supplied by dynamic root water uptake. *J. Adv. Model. Earth Syst.*, **12**, e2020MS002062, https://doi.org/10.1029/2020MS002062.

Otkin, J. A., M. C. Anderson, C. Hain, I. E. Mladenova, J. B. Basara, and M. Svoboda, 2013: Examining rapid onset drought development using the thermal infrared–based evaporative

stress index. *J. Hydrometeor.*, **14**, 1057–1074, https://doi.org/10.1175/JHM-D-12-0144.1.

——, and Coauthors, 2016: Assessing the evolution of soil moisture and vegetation conditions during the 2012 United States flash drought. *Agric. For. Meteor.*, **218–219**, 230–242, https://doi.org/10.1016/j.agrformet.2015.12.065.

Ozdogan, M., M. Rodell, H. K. Beaudoing, and D. L. Toll, 2010: Simulating the effects of irrigation over the United States in a land surface model based on satellite-derived agricultural data. *J. Hydrometeor.*, **11**, 171–184, https://doi.org/10.1175/2009JHM1116.1.

Peters-Lidard, C. D., and Coauthors, 2007: High-performance Earth system modeling with NASA/GSFC's Land Information System. *Innov. Syst. Software Eng.*, **3**, 157–165, https://doi.org/10.1007/s11334-007-0028-x.

Poltoradnev, M., J. Ingwersen, K. Imukova, P. Högy, H. Wizemann, and T. Streck, 2018: How well does Noah-MP simulate the regional mean and spatial variability of topsoil water content in two agricultural landscapes in southwest Germany? *J. Hydrometeor.*, **19**, 555–573, https://doi.org/10.1175/JHM-D-17-0169.1.

Sabater, J. M., C. Rüdiger, J.-C. Calvet, N. Fritz, L. Jarlan, and Y. Kerr, 2008: Joint assimilation of surface soil moisture and LAI observations into a land surface model. *Agric. For. Meteor.*, **148**, 1362–1373, https://doi.org/10.1016/j.agrformet.2008.04.003.

Sawada, Y., T. Koike, E. Ikoma, and M. Kitsuregawa, 2020: Monitoring and predicting agricultural droughts for a water-limited subcontinental region by integrating a land surface model and microwave remote sensing. *IEEE Trans. Geosci. Remote Sens.*, **58**, 14–33, https://doi.org/10.1109/TGRS.2019.2927342.

Sheffield, J., Y. Xia, L. Luo, E. F. Wood, M. Ek, and K. E. Mitchell, 2012: North American Land Data Assimilation System: A framework for merging model and satellite data for improved drought monitoring. *Remote Sensing of Drought: Innovative Monitoring Approaches*, B. Wardlow, M. C. Anderson, and J. P. Verdin, Eds., CRC Press, 484 pp., https://doi.org/10.1201/b11863.

——, and Coauthors, 2014: A drought monitoring and forecasting system for sub-Sahara African water resources and food security. *Bull. Amer. Meteor. Soc.*, **95**, 861–882, https://doi.org/10.1175/BAMS-D-12-00124.1.

Svoboda, M., and Coauthors, 2002: The Drought Monitor. *Bull. Amer. Meteor. Soc.*, **83**, 1181–1190, https://doi.org/10.1175/1520-0477-83.8.1181.

Tian, S., A. I. J. M. Van Dijk, P. Tregoning, and L. J. Renzullo, 2019: Forecasting dryland vegetation condition months in advance through satellite data assimilation. *Nat. Commun.*, **10**, 469, https://doi.org/10.1038/s41467-019-08403-x.

Ukkola, A. M., M. G. De Kauwe, A. J. Pitman, M. J. Best, G. Abramowitz, V. Haverd, M. Decker, and N. Haughton, 2016: Land surface models systematically overestimate the intensity, duration and magnitude of seasonal-scale evaporative droughts. *Environ. Res. Lett.*, **11**, 104012, https://doi.org/10.1088/1748-9326/11/10/104012.

Xia, Y., and Coauthors, 2012: Continental-scale water and energy flux analysis and validation for the North American Land Data Assimilation System project Phase 2 (NLDAS-2), 1: Intercomparison and application of model products. *J. Geophys. Res.*, **117**, D03109, https://doi.org/10.1029/2011JD016048.

——, M. B. Ek, D. M. Mocko, C. D. Peters-Lidard, J. Sheffield, J. Dong, and E. F. Wood, 2014: Uncertainties, correlations, and optimal blends of drought indices from the NLDAS multiple land surface model ensemble. *J. Hydrometeor.*, **15**, 1636–1650, https://doi.org/10.1175/JHM-D-13-058.1.

Xiao, Z., S. Liang, J. Wang, Y. Xiang, X. Zhao, and J. Song, 2016: Long-time-series global land surface satellite leaf area index product derived from MODIS and AVHRR surface reflectance. *IEEE Trans. Geosci. Remote Sens.*, **54**, 5301–5318, https://doi.org/10.1109/TGRS.2016.2560522.

Yan, H., and H. Moradkhani, 2016: Combined assimilation of streamflow and satellite soil moisture with the particle filter and geostatistical modeling. *Adv. Water Resour.*, **94**, 364–378, https://doi.org/10.1016/j.advwatres.2016.06.002.

Yang, Z.-L., and Coauthors, 2011: The community Noah land surface model with multiparameterization options (Noah-MP): 2. Evaluation over global river basins. *J. Geophys. Res.*, **116**, D12110, https://doi.org/10.1029/2010JD015140.